REPORT DOCUMENTATION PAGE

Form Approved
OMB No. 0704-0188

1. REPORT DATE *(DD-MM-YYYY)*	**2. REPORT TYPE**	**3. DATES COVERED** *(From - To)*
May 2013	Technical Paper	May 2013-June 2013

4. TITLE AND SUBTITLE
Impact of excitation and reaction processes on FRC thruster efficiency

5a. CONTRACT NUMBER
In-House

5b. GRANT NUMBER

5c. PROGRAM ELEMENT NUMBER

6. AUTHOR(S)
Brackbill, Gimelshein, Gimelshein, Cambier

5d. PROJECT NUMBER

5e. TASK NUMBER

5f. WORK UNIT NUMBER
Q02Z

7. PERFORMING ORGANIZATION NAME(S) AND ADDRESS(ES)

Air Force Research Laboratory (AFMC)
AFRL/RQRS
1 Ara Drive.
Edwards AFB CA 93524-7013

8. PERFORMING ORGANIZATION REPORT NO.

9. SPONSORING / MONITORING AGENCY NAME(S) AND ADDRESS(ES)
Air Force Research Laboratory (AFMC)
AFRL/RQR
5 Pollux Drive
Edwards AFB CA 93524-7048

10. SPONSOR/MONITOR'S ACRONYM(S)

11. SPONSOR/MONITOR'S REPORT NUMBER(S)
AFRL-RQ-ED-TP-2013-120

12. DISTRIBUTION / AVAILABILITY STATEMENT
Distribution A: Approved for Public Release; Distribution Unlimited. PA#13276

13. SUPPLEMENTARY NOTES
Conference paper for the 44th AIAA Thermophysics Conference, San Diego, CA, June 2013.

14. ABSTRACT
The paper focuses on numerical simulation of neutral entrainment in a Field Reversed Configuration thruster with a neon propellant. A fully kinetic approach based on a Particle-In-Cell method of modeling plasmas and the Direct Simulation Monte Carlo method of modeling neutrals is applied. An implicit PIC code Celeste3D extended to compute neutral transport and collision processes between neutral and charged particles are used. The current collision model includes all key elastic, collisional radiative, and reaction processes in neon. Temporal evolution of gas and plasma macroparameters and thruster performance properties is presented.

15. SUBJECT TERMS

16. SECURITY CLASSIFICATION OF:			**17. LIMITATION OF ABSTRACT**	**18. NUMBER OF PAGES**	**19a. NAME OF RESPONSIBLE PERSON**
					Jean.Luc Cambier
a. REPORT	**b. ABSTRACT**	**c. THIS PAGE**	SAR	13	**19b. TELEPHONE NO** *(include area code)*
Unclassified	**Unclassified**	**Unclassified**			661-525-5649

Standard Form 298 (Rev. 8-98)
Prescribed by ANSI Std. 239.18

Impact of Excitation and Reaction Processes on the Field Reversed Configuration Thruster Efficiency

Jeremiah Brackbill* and Natalia Gimelshein*
and Sergey Gimelshein*
ERC, Inc., Edwards AFB, CA 93524

Jean-Luc Cambier†
Air Force Research Laboratory, Edwards AFB, CA 93524

The paper focuses on numerical simulation of neutral entrainment in a Field Reversed Configuration thruster with a neon propellant. A fully kinetic approach based on a Particle-In-Cell method of modeling plasmas and the Direct Simulation Monte Carlo method of modeling neutrals is applied. An implicit PIC code Celeste3D extended to compute neutral transport and collision processes between neutral and charged particles is used. The current collision model includes all key elastic, collisional radiative, and reaction processes in neon. Temporal evolution of gas and plasma macroparameters and thruster performance properties is presented.

I. Introduction

High-power electric propulsion is an enabling technology for future space missions, but one that also presents a number of technical challenges. First, it is critically important to operate a thruster at very high efficiency, otherwise the system limitations due to heat rejection become insurmountable. Second, high power can be efficiently delivered into a plasma by raising its temperature (provided radiative losses are not excessive), i.e. its specific energy; consequently, the specific impulse can take large values, even in the excess of 10,000 sec. The optimal conditions from the standpoint of low radiation loss, acceptable ionization cost, and confinement requirements, are usually achieved for low-Z plasma at high (50-100 eV) temperature and in strong magnetic fields. These conditions are typically obtained in Field Reversed Configuration (FRC) (see, for example, Ref. 1) plasma. The FRC is a self-organized magnetized plasma structure in the shape of a highly compact toroid. The magnetic field is mostly in the poloidal direction,[2] generated by internal (toroidal) currents. The ratio of plasma pressure to magnetic pressure is close to unity, i.e. the highest plasma density that can be attained for given external magnets. The poloidal field also contributes to the particle confinement. Starting from a background uniform plasma at a constant axial (bias) field, the FRC can be formed by pulsing external coils and reversing the applied field, inducing currents at the plasma boundary and "pinching" the plasma at both ends (see Fig. 1). The initial bias field is trapped inside the plasma and forced to reconnect at the end points (separatrix), creating an elongated toroidal shape.

In contrast to some other high I_{sp} plasma propulsion concepts,[3] the FRC is completely magnetically insulated from the external field: the plasma is not tied to an external field line, and the FRC can readily detach from the confining external field. It can also be translated and accelerated by applying a gradient of magnetic pressure using pulsed external coils. The FRC can therefore be efficiently accelerated to provide thrust, operates at a temperature that is optimal for ionization and is well confined. The basic concept of operations has been demonstrated[4] and more recent research has led to further optimization of the formation process,[5] while methods for increased efficiency through energy recovery in the electrical circuits are currently being developed. One of the latest design iterations[6] provides plasma velocities in the 10-40 km/sec range,

*Consultant
†Senior Scientist, Propulsion Directorate

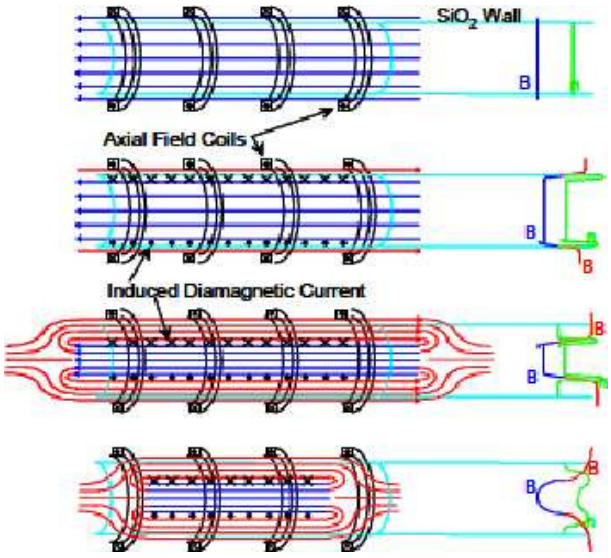

Figure 1. Schematic of basic FRC formation by field reversal.

a desirable regime for USAF applications. However, many aspects of the flow development and device operation, such as power and mass utilization efficiencies, still remain to be determined more precisely.

One of the key features of a versatile FRC thruster is its ability to increase thrust level and operational efficiency through the process of entrainment of neutral (and possibly ambient) gas by a translating FRC plasmoid. The main idea of such an entrainment is the interaction of fast ions with slow neutrals, subsequent charge exchange reactions, and the creation of slow ions and fast neutrals. Fast neutrals will then exit the thruster and produce thrust, while slow ions may again be accelerated. The repetition of this process will allow drastic reduction of energy loss on ionization, while gaining thrust through multiple collisions of accelerated ions with slow neutrals. A significant problem that may reduce the usefulness of the neutral entrainment is the electron impact ionization reactions. These reactions may not just reduce the benefits of entrainment, but potentially diminish its usefulness.

In recent paper,[7] chemical reactions between ions and electrons of a translated at high velocities field reversed plasmoid and neutral gas particles were examined. Importance of different reaction mechanisms, such as charge exchange and electron impact ionization, was analyzed for conditions typical for FRC thrusters. Then, an implicit Particle-In-Cell code, Celeste3D,[8] extended to include plasma-neutral and neutral-neutral elastic and inelastic processes and Coulomb collisions, was used to model a planar flow between an FRC plasmoid initially at a Schmid-Burgk equilibrium, and neutral gas with varying relative velocities, plasma temperatures, and neutral gas densities. The contribution of charge exchange and electron impact ionization reactions was analyzed, and the sensitivity of the entrainment efficiency to the plasmoid translation velocity and neutral density was evaluated.

In the present work, which is the continuation of our previous effort,[7] the focus is on (i) implementing the electronic excitation processes and (ii) analysis of thruster efficiencies for a neon FRC plasmoid with various plasma temperatures. Efficiency of using local gas injection is evaluated, and the limits of thrust increase through the neutral density variation are examined. In the next section, the proposed model for collisional radiative processes in neutral entrainment of a neon plasmoid is presented. Then, the collisional relaxation in a spatially homogeneous thermal bath is studied. Finally, the implementation of collision processes to Celeste3D and modeling of a 2D FRC neutral entrainment is discussed.

II. Collisional radiative and reacting processes in neon neutral entrainment

The main focus of this work is on neon propellant, since it appears to benefit from high ionization threshold, and thus relatively low losses due to ionization in collisions between hot electrons of the plasmoid and cold neutrals of the entraining gas.[7] Xenon, which may be attractive due to its high mass, has much

lower ionization threshold, and the associated energy losses may significantly decrease the entrainment efficiency. Helium, conversely, is difficult to ionize but its low mass make it poor propellant. In the first work where kinetic modeling was used to analyze the plasmoid translation and neutral entrainment,[7] the reaction processes between a neon plasmoid and neutral gas included only the charge exchange and electron impact ionization reaction. The electronic excitation, and the resulting loss of plasmoid energy to radiation, was not considered, even though it is an important process with a rate exceeding that of the electron impact ionization at plasma temperatures of about or below 5 eV. In the present work, all key relaxation and reaction processes are included in the model.

The following neon states are known to exist in a neon plasma:

1. Neutral atoms in the ground electronic state,
2. Neutral atoms in metastable states with lifetimes in tens of seconds (effectively infinite on a sub-millisecond scale of the FRC entrainment process),
3. Neutral atoms in resonant states that quickly decay into ground state (such a decay is typically fast enough to be considered instantaneous),
4. Neutral atoms in non-resonant excited states with short radiative lifetimes (14.5-27 ns).[9] From these states, the atoms may radiatively decay either to a metastable or a resonant state.
5. Positively charged ions (only singly charged ions need to be considered in a low-Z FRC thruster environment).

The lifetimes of resonant and non-resonant states are typically in tens of nanoseconds, while the characteristic time of neutral entrainment, which is the time it takes an FRC plasmoid moving at about 20 km/s to pass through the neutral field, is in tens of microseconds. Therefore, it may be assumed without any loss of accuracy that the resonant and non-resonant states emit photons immediately after the corresponding collision, and thus the collision/reaction process is reduced to the energy loss of the colliding particle pair. That means that in the kinetic model, only three states need to be considered: neutral atoms, metastable atoms, and ions. Since neon has two metastable levels with closely spaced energies (16.619 eV and 16.716 eV), those can be effectively lumped together without any noticeable loss of accuracy. The resulting model appears as follows.

Part I: Elastic collision processes

- Neon ground state atom elastic collisions with electrons. The cross-sections for high energy elastic collisions are taken from Ref. 10, 11, and the values for low impact energies are taken from Ref. 12.
- Elastic collisions between neutral atoms. The variable hard sphere model with parameters from Ref. 13 is applied for this interaction.
- Coulomb collisions between charged particles. The model[14] is implemented to compute these collisions.

Part II: Plasmachemical reactions:

- Charge exchange reactions. Similar to the previous work,[7] the charge exchange reaction cross section of Ref. 15 is used here. The after-collision velocities of the colliding ion and neutral are swapped.
- Elastic collisions between neutrals and electrons. The cross section for this process was assumed to be one-half of the charge exchange cross section, according to the recommendation of Ref. 15.

Part III: Collision radiative processes

- Electron impact ionization of ground state atoms, $\mathrm{Ne} + e \rightarrow \mathrm{Ne}^{+} + e + e$. For this reaction, the cross sections from SIGLO database[16] are used in the computations.
- Electron impact excitation of ground state atoms to metastable states, $\mathrm{Ne} + e \rightarrow \mathrm{Ne}^{*}_{M} + e$. The cross-sections for this process are taken from Ref. 17.

- Electron impact excitation from the ground state to a short-lived excited state, followed by radiative decay into either metastable or resonance state. Since the resonance state is short-lived, and the cross-section for the excitation to metastable state already takes into account the cascade contributions from higher levels, the product of this reaction should be a ground-state atom, Ne $+e \rightarrow$ Ne$+e+h\nu$. In this work, the cross sections recommended in Ref. 18 are used.

- Electron impact excitation of ground state atoms to resonant states, followed by the radiative decay to the ground state, Ne $+e \rightarrow$ Ne$+e+h\nu$. For this process, the cross-section are taken from Ref. 19.

- Transition of metastable atoms to resonant states, with the subsequent de-excitation, $Ne^*_M+e \rightarrow$Ne$+e+h\nu$. The rate constant for this process is equal to $2 \cdot 10^{-7}$ cm^3/s,[20] and the cross-sections for kinetic modeling are calculated using the total collision energy model.[21]

- Electron impact ionization of metastable atoms, $Ne^*_M + e \rightarrow Ne^+ + e + e$. The cross sections for this process are taken from Ref. 22.

- Electron impact excitation of metastable atoms to non-resonant exited states, $Ne^*_M + e \rightarrow Ne^* + e$. Since the products of this reaction are short-lived, the reaction product is a ground-state atom. The reaction cross-sections follow from Ref. 18.

Due to the lack of detailed, differential collision cross sections for most of the above processes, an isotropic scattering is assumed to calculate after-collision velocities of atoms and electrons in all interactions with the exception of Coulomb collisions and charge exchange reactions. This assumption is not expected to significantly impact the results presented in the following sections.

III. Collisional relaxation of plasma and neutral gas in 0D heat bath

Consider first the impact of the plasmoid temperature on the time evolution of plasma and neutral properties in an adiabatic heat bath with key macroscopic properties, such as relative velocity between neutrals and plasma, and plasma temperature, that correspond to conditions typical for an FRC thruster. It is assumed that the neutral and charged species, initially at equilibrium at their respective temperatures, have a relative velocity of 20 km/s between them; due to the symmetry of the problem, the average plasma velocity of 0 and neutral velocity of 20 km/s is assumed. The initial neutral temperature is 10 K, and the plasma temperature is either 5 eV or 10 eV; both neutral and plasma density are 10^{18} m^{-3}. To simulate the neutral entrainment process, a 0D direct simulation Monte Carlo (DSMC) code was developed that incorporates all processes listed in the previous section.

The temperature profiles of neutrals (T_n), ions (T_i), and electrons (T_e) as a function of time are shown in Fig. 2 (left) for an initial plasma temperature of 5 eV. During the first few microseconds, there are not enough ionization reactions for the electron temperature to noticeably change. At the same time, the high-energy elastic collisions between neutrals and ions (their relative collision velocity of 20 km/s corresponds to an energy of 20 eV, and thus a temperature of about 10 eV) result in the increase in both ion and neutral temperature. The maximum ion and neutral temperature of about 9 eV is reached at about 100 μs. Note that the maximum value is impacted by the ionization and radiation losses, that start to contribute after about 10 μs. The electron temperature does not have a visible maximum due to relatively slow relaxation on heavy particles, and also due to energy losses to the electronic excitation / radiation and ionization. The relative contribution of the ionization and the collisional radiative processes is illustrated in Fig. 2 through the simulation of the plasma/neutral interaction with only the charge exchange and electron impact ionization included (the corresponding electron temperature is labeled "T$_e$ no CR"). It is clear that the collisional radiation is more important for the relatively low temperature of 5 eV than the ionization processes, as it is responsible for over 70% of the electron temperature decrease. By the time of 1 ms, about three percent of electrons and neutrals have participated in ionization.

The temperature evolution for a hotter plasma is qualitatively similar to 5 eV, but the impact of the radiation and ionization is much more pronounced in this case due to the increased rates of these processes. After 1 ms, the electron temperature decreases by almost 60%, as about 15% of electrons and neutrals participated in electron impact ionization.. Most of that decrease is due to the ionization, as the corresponding temperature for the no-excitation case is about 50% of the initial temperature. Similar to the 5 eV case, the neutral and ion temperatures increase over the first 100 μs, and then decrease due to the excitation

and ionization. It is important to note that for both initial plasma temperatures there is a strong thermal non-equilibrium, with the species temperatures significantly different due to the elastic and inelastic collision processes.

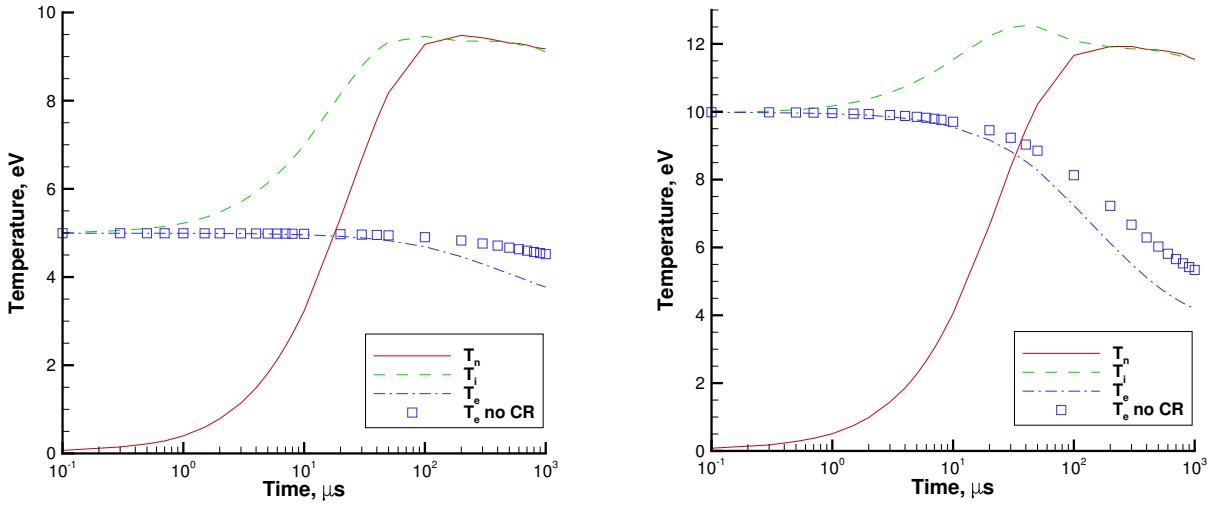

Figure 2. Species temperature relaxation for initial plasma temperature of 5 eV (left) and 10 eV (right).

The non-equilibrium is manifested not only at the macroscopic level with the species temperature difference, but also at the microscopic level of the velocity distribution functions. The distribution functions of ion velocities in the direction of neutral-plasma relative velocity at different time moments are shown in Fig. 3 (left). Initially Maxwellian (Gaussian) distribution becomes clearly bimodal after the first few microseconds. The peak at the 20 km/s corresponds to ions that participated in charge exchange reactions and thus acquired the velocity of neutrals. The bimodality essentially disappears after about 50 μs, but the ion distribution function is still visibly non-Maxwellian even after 1 ms. The neutral atom distribution function (not shown here) is also non-equilibrium, and qualitatively similar to that of ions. The non-equilibrium in the velocity distribution functions shows the importance of using a kinetic approach for modeling FRC neutral entrainment, since a continuum approximation would typically undepredict (and in some cases over-predict) the actual reaction rates.

The electron velocity distribution function is fairly close to equilibrium throughout the relaxation process, as illustrated in Fig. 3 (right) for a time moment of 1 ms. The distribution function profile is nearly Maxwellian both for the baseline model that includes all interaction types, and the model that does not take into account the excitation processes. The change in shape between the two models corresponds to the temperature difference between them discussed earlier (see fig. 2, left). It is important to note that the principal mechanism responsible for the equilibration of the electron velocity distribution function is electron-electron Coulomb collisions. The distribution function obtained in a simulation that does not include these collisions is also presented in Fig. 3 (right); it shows a significant depletion of high velocity tails of the distribution function. As a result, ignoring Coulomb collisions would strongly decrease the number of electronic excitations and electron impact ionizations.

IV. Numerical approach and flow conditions for 2D FRC entrainment

Modeling of the interaction between an FRC plasmoid and the entraining gas is conducted in this work with an implicit three-dimensional PIC code Celeste3D that solves the full set of Maxwell-Vlasov equation and has been extensively used in the past for various astrophysical and laboratory plasma problems.[23,24] The implicit moment formulation of the PIC method implemented in Celeste results in highly efficient simulations based on ion length and time scales, and not electron scales as explicit methods do, while retaining the kinetic effects of both the electrons and the ions. An explicit simulation requires the time step to be $\Delta t < 2/\omega_{pe}$, and the spatial cell size to be $\Delta x < \zeta\lambda_e$ in order to avoid the finite grid instability. Here, ω_{pe} is the electron plasma frequency, and λ_e is the electron Debye length. In an implicit simulation, these requirements are

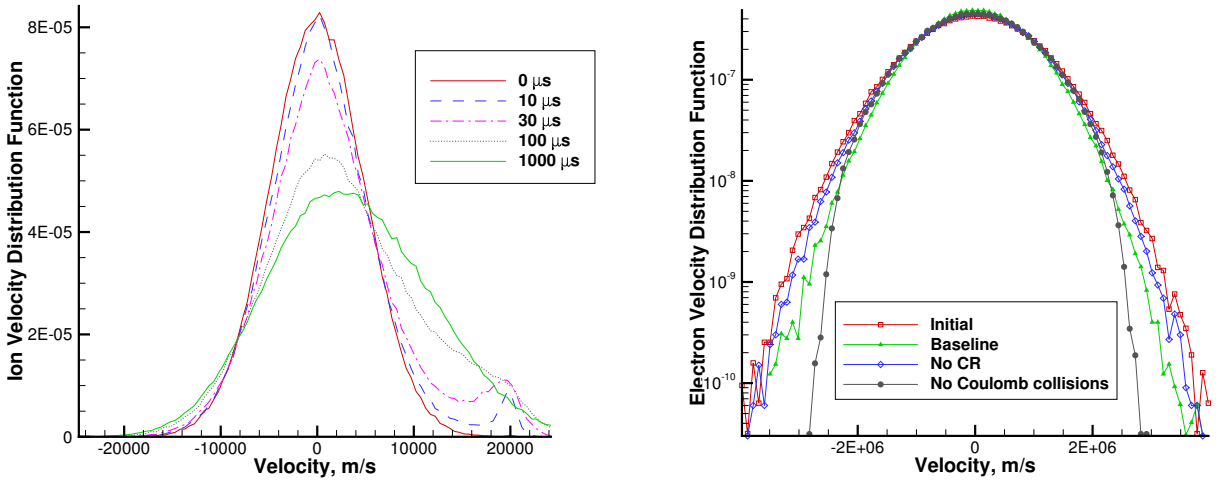

Figure 3. Ion velocity distribution function as a function of time (left). Electron velocity distribution function at 1 ms (right). The initial plasma temperature of 5 eV.

replaced by an accuracy condition related to the conservation of energy, $\Delta t < frac\Delta xc_e$, where c_e is the electron thermal speed.

The original Celeste3D models the evolution of ion and electron populations as described by the Vlasov equation, coupled with the solution of full Maxwell equations; it does not simulate neutral particles. To study the neutral entrainment process, Celeste3D was extended in the previous work[7] to include neutral transport and collisional relaxation. A Direct Simulation Monte Carlo based capability has been added to Celeste that models neutral transport and collisions. The collision processes included in the present model are discussed in Section II. As all species have different weights, a weighting scheme[25] is applied. The majorant collision frequency[26] of the DSMC method is used to simulate the collision process in cells.

Although the actual entrainment geometry is three-dimensional, as a nearly axisymmetric plasmoid interacts with neutral gas supplied from two or more azimuthal injectors, three-dimensional PIC modeling is extremely time consuming, and in this work it was replaced by a 2D (planar flow). The result is a much larger number of particles per cell and thus smaller statistical scatter. The grid was 40×80, and the number of simulated ions, electrons, and neutrals per cell was approximately 64, 100, and 512, respectively. Since the cost of an implicit simulation is a direct function of the electron mass (see above, the computational time is inversely proportional to the square root of the electron mass m_e), the simulation efficiency may be further enhanced through the introduction of the weighted electron mass, $m'_e = Wm_e$, where the constant $W > 1$. The ion-to-electron mass ratio has to be high enough to preserve the kinetic effects, and the value of m_i/m'_e on the order of 100 is usually sufficient.[23] In this work, $m_i/m'_e = 100$ is used (modeling of the baseline case of a 5 eV plasmoid with a neutral entrainment for a ratio of $m_i/m'_e = 300$ have shown identical results). The initial conditions used to set an equilibrium plasmoid is the a Schmid-Burgk equilibrium[27] with the average plasma density of 10^{18} m^{-3} and two plasma temperatures of 5 and 10 eV. In all computations, the size of the computational domain

To simplify the inflow boundary conditions, the neutral-plasma interaction is examined in the reference frame of the plasmoid, so that the neutral gas is injected into the computational domain from the left boundary, and then passes through the domain from left to right. The properties of the injected neutral gas are changed to study their impact on the neutral-plasma interaction. The difference from the previous work,[7] in addition to a much more complete collisional relaxation model, is the local injection of neutrals. While in the previous work the neutrals were introduced from the entire left boundary, here the neutrals are injected only in the central part of the flow (the injection area was 0.02 m). This allows one to to study the trajectories of the after-collision atoms, and analyze the usability of local injection concept.

In all computations, open boundary conditions for neutrals and plasma were imposed at the left and right boundaries, and a conducting wall with specular reflection was set at the top and bottom boundaries. Note that computations were also performed with no neutral inflow to analyze the temporal evolution of the plasmoid; it was observed that the equilibrium is maintained for at least 10,000 ion plasma periods. This amounts to over 30 μs for the conditions under consideration, and is longer than the plasmoid-neutral

interaction time. The macroparameters presented below are the result of an instantaneous average (ensemble sampling) of gas and plasma properties over cells. The distribution functions of neutral atom velocities were also ensemble averaged. The thrust force was calculated in this work by an integration over a cross section that moves with a velocity equal to that of the neutral gas. An axial symmetry around the lower boundary is assumed in the integration in order to provide the link between the computed force and the actual FRC thruster.

The schematics of the numerical setup is illustrated in Fig. 4 where the ion and neutral densities are shown at time $t = 8$ μs. Hereafter, $t = 0$ corresponds to the initial state when the neutral gas starts to flow into the computational domain. At $t = 8$ μs, the injected at $X = 0$ within $0.09 < Y < 0.11$ m neutrals have crossed slightly more than half of the domain. The neutral bulk velocity in X direction is 20 km/s, much higher than the average thermal velocity of about 0.1 km/s, and thus the divergence of the flow is fairly small. Neutrals that appear outside the $0.09 < Y < 0.11$ m region have traveled there after being scattered as a result of ion-neutral collisions. The ion density is maximum at the center of the domain, and that is the region that affects neutrals most.

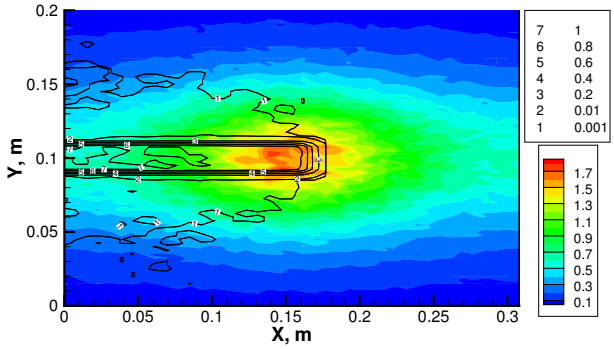

Figure 4. FRC neutral entrainment setup. Field: ion number density (10^{18} m^{-3}), isolines: neutral gas number density (10^{18} m^{-3}).

V. FRC neutral entrainment results

The time-dependent evolution of neutral gas penetrating the plasmoid is given in Fig. 5, left, where the gas density is shown for two initial plasma temperatures of 5 and 10 eV and three time moments, $t = 0.08$, 8, and 16 μs. After the first microsecond, there is no visible change of neutral gas density from its free stream value. As neutral gas starts to penetrate denser plasma region, some scattering of neutrals to the side is observed. However, after the neutral jet passed through the plasmoid center, there is still no neutrals at the walls of the FRC chamber, primarily because there was not enough time for reflected neutrals to reach them. The average thermal velocity of neutrals after collisions with ions corresponds to the temperature of the plasmoid, and this is about 7 km/s for 5 eV and about 10 km/s for 10 eV. After the neutral gas passed through the plasmoid ($t = 16$ μs), the reflected neutrals reach the chamber walls, but there density in that region is fairly small, up to three orders of magnitude smaller than that in the coreflow. This is a combined effect of relatively small number of collisions that mostly occur in the center of the plasmoid, lower after-collision neutral velocities, and the preferential direction of these velocities (aligned with neutral jet). Note that the impact of plasmoid temperature on neutral density is relatively small, as only a few percent smaller number of neutrals reaches the right boundary for 10 eV. This few percent loss is primarily attributed to electron impact ionization reactions.

The evolution of ion number density for two plasmoid temperatures as the result of the neutral-plasma interaction is shown in Fig. 5, right. The change in ion density during the first 8 μs is small, and related mostly to the statistical perturbations and some minor change in density distribution as the plasmoid slightly deviates from the Schmid-Burgk equilibrium, and not to the entrainment process. The only neutral-related change at that time is noticeable in the plasmoid coreflow. The change between the 8 μs and 16 μs fields is more significant. As expected, it is observed only in the coreflow, the region where the neutral jet passes through. At 5 eV, the number of ionization reaction is much smaller than at 10 eV, and thus the neutral

entrainment is less pronounced. At 10 eV, the ion density in the coreflow increases by up to 10% with respect to the initial equilibrium values. There is also some momentum transfer from neutral jet to the plasmoid, as the latter visibly shifts to the right at $t = 16$ μs.

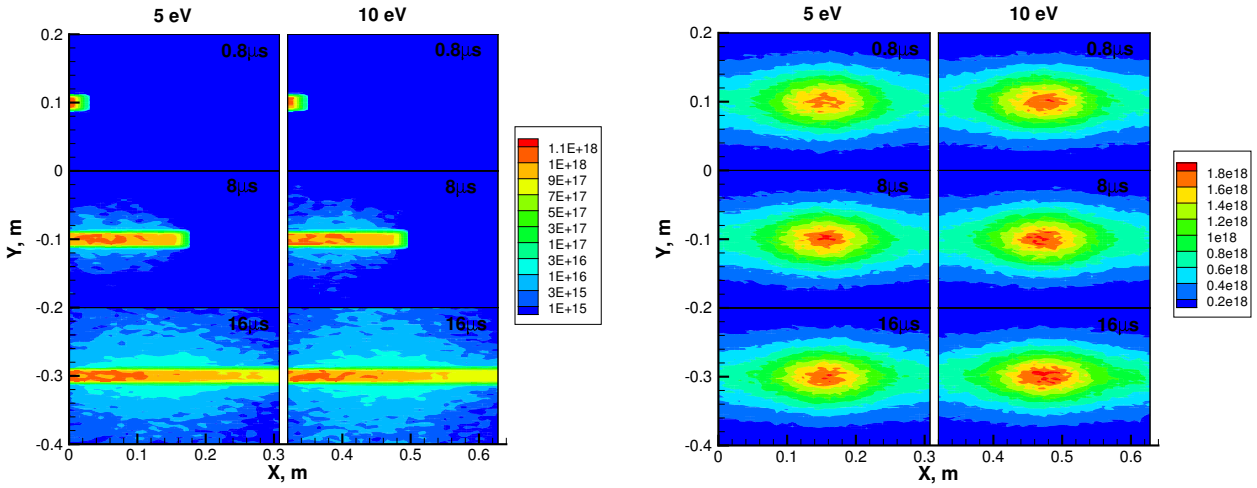

Figure 5. Neon number density (m^{-3}), left, and ion density (m^{-3}),right, for 5 eV (left columns) and 10 eV (right columns) at different time moments since the injection. Injected neutral density is 10^{18} atom/m^3.

As follows from Fig. 5, left, the number of neutrals that reach the right boundary of the computational domain for the neutral jet density of 10^{18} atom/m^3 is about 87% and 85% for 5 eV and 10 eV plasmoids, respectively. Since the number density of neutrals is close to the average number density of the plasmoid, that implies that only on the order of 10% of the plasma particles had collisions with neutrals. There are two obvious ways to increase that number: (i) increase the interaction time, or (ii) increase neutral density. The first approach is not efficient since it requires either decreasing the plasmoid velocity, and thus will reduce the thruster specific impulse, or increasing the thruster size. The second approach may be more beneficial, especially remembering that in the actual thruster, the pulsed mode of the fast plasmoid along with low velocities of neutrals may allow for a multi-pass entrainment of neutrals. In order to analyze the impact of higher neutral density, the computations were conducted for densities that are 5 and 25 times higher than the baseline of $n = 10^{18}$ atom/m^3.

The neutral density field for $n = 2.5 \times 10^{19}$ atom/m^3 at different time moments is shown in Fig. 6, left, for the two plasmoid temperatures under consideration. Qualitatively, the plot looks similar to that for the 25 time lower neutral density. No significant deflection is noticeable after the first microsecond after the injection; at 8 μs, there is a noticeable amount of neutrals scatter to the side, although none of those have reached the chamber walls yet. At 16 μs, the neutrals reflected after collisions with ions reach the chamber, although their density near the wall is full three orders of magnitude smaller than in the coreflow. More importantly, almost 12% of neutral particles collide with plasma particles as the neutral jet crosses the 5 eV plasmoid; for a 10 eV plasmoid, this number reaches 15%, similar to the lower density case.

Since the neutral density is much higher than that of the plasmoid, one can expect significant entrainment in this case. And this is indeed the case, as Fig. 6, right, clearly shows. There is a significant increase of plasma density even at $t = 8$ μs. At that time, the ion and electron density in the center of the plasmoid is over 50% higher than the corresponding equilibrium value for the 5 eV plasmoid, and is almost two times higher for the higher temperature of 10 eV. Note that such a difference between 5 eV and 10 eV is consistent with the temperature dependence of the electron impact ionization reaction.[7] Further interaction between the plasmoid and neutral gas ($t = 16$ μs) results in a lower maximum plasma density that for $t = 8$ μs. This is related primarily to the neutral-to-plasma momentum transfer. At $t = 16$ μs, the plasmoid loses its equilibrium ellipsoidal shape, and significant part of it translates with the neutrals. This is due to charge exchange and, to a lesser extent, elastic collisions, both of with transfer the X momentum to ions. While the total number of plasma particles is significantly larger at 16 μs than at 8 μs, this number is spread over significant distance.

The neutral entrainment also results in significant increase of ion temperature, discussed in detail in the

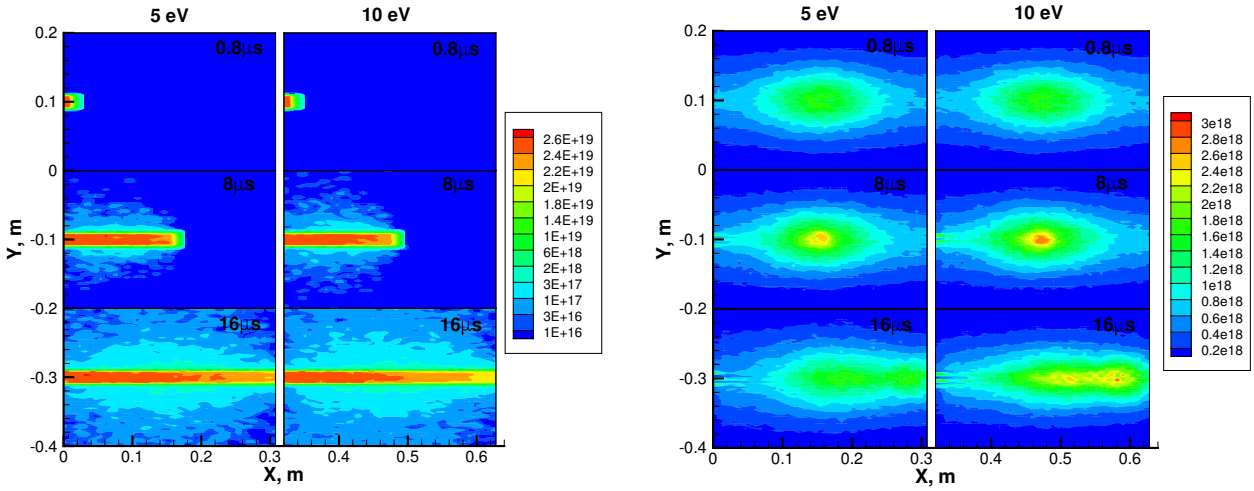

Figure 6. Same as Fig. 5, for neutral density of 25×10^{18} atom/m^3.

previous section. Due to highly energetic elastic collisions between neutrals and ions (the average collision energy is about 40 eV), as well as charge exchange reactions that increase ion velocities to 20 km/s, the ion temperature increases to almost 10 eV when the initial plasmoid temperature was 5 eV, and to over 13 eV for the 10 eV plasmoid, as shown in Fig. 7, left. This result is consistent with the earlier Fig. 2. Note also that at 16 μs the high ion temperature region splits in two parts, above and below the domain symmetry axis, which is attributed to the plasmoid translation and ion mixing in these regions. The computations show that the electron temperature (not shown here) is practically not affected by the plasmoid entrainment during the plasma-neutral interaction. Due to the low rate of momentum and energy transfer in the electron-heavy particle collisions, the electron temperature does not change in the computations by more than a few percent (decreases by about 5% for a 10 eV plasmoid). This result is also in line with what was observed earlier in the homogeneous heat bath relaxation.

All plasma and neutral species are in thermal nonequilibrium, which is manifested in differences in their translational temperatures as well as in non-Maxwellian distribution functions. The elector and ion velocity distribution in the 2D FRC entrainment are similar to those considered in the previous section, so here we only present the distribution function of X component velocity for neutral atoms. The velocity distribution function of neutrals is shown in Fig. 7, right. Since single-cell transient results have considerable noise, the average of all cells is presented in this figure. Note that the velocity distributions weakly depend on the neutral gas density, and thus only the case of 10^{18} atom/m^3 is given here. As clearly seen in Fig. 7, right, the neutral velocity is bimodal, with a sharp peak at -20 km/s corresponding to the injected atoms that did not have any collisions with plasma, and the second, much lower maximum, at $U = 0$ corresponding to the atoms collided with ions. Fairly quick equilibration after collisions with the isotopic scattering results in the second maximum having a shape of a Maxwellian distribution with the corresponding plasma temperature. This is illustrated by comparison with the Mott-Smith bimodal solution with the mode temperatures of 10 K and 10eV. The ratio of collided to non-collided neutrals is approximately 0.1 for both plasmoid temperatures.

Consider now the contribution of different gas and plasma species to the thrust force, illustrated in Fig. 8 for a 5 eV plasmoid and a neutral density of 10^{18} atom/m^3. In this figure, p denotes the contribution of the pressure component (thermal motion of particles) of the corresponding species, and ρU^2 denotes the contribution of the momentum component (translational motion). The momentum component of the electrons, as well as pressure component of the neutral gas, are negligible and thus not plotted here. The next important contributors are ion and electron pressures, which almost coincide in the considered case; their combined effect amounts at its peak to about 10% of the total thrust force.

It is important to remember that there are several key differences of the considered setup from an actual operating FRC thruster. First, the reference frame of the plasmoid is chosen in the computations. Second, the numerical simulation is two-dimensional. Third, and probably most important, the modeling lacks an accelerating magnetic field. Such a field would transfer momentum to the plasmoid, and replenish the momentum loss caused by the collisions with the neutrals. As the result of the latter numerical approximation,

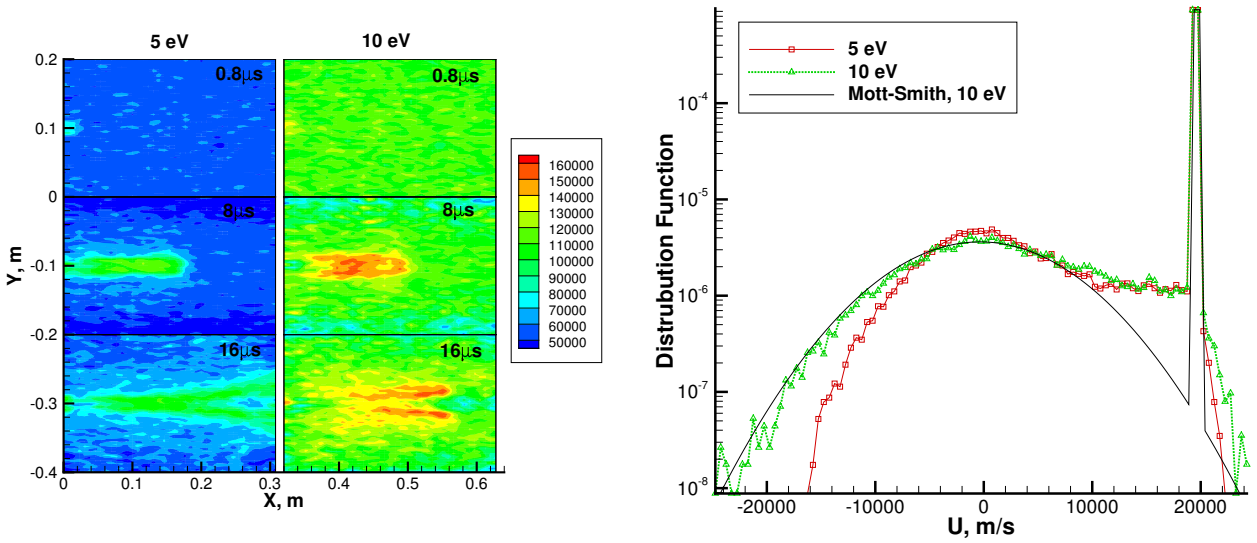

Figure 7. Left: ion translational temperature at different time moments for neutral density of 25×10^{18} atom/m^3. Right: neutral velocity distribution function at $t = 16$ μs for neutral density of 10^{18} atom/m^3.

and due to the conservation of mass, momentum, and energy in the numerical modeling, the total thrust force computed over neutral and plasma species does not change when the physical model or flow conditions are modified. The indication of the entrainment efficiency is therefore the amount of energy and momentum transferred from plasma (primarily ion) species to the neutrals. The larger the decrease in thrust force produced by the ions, the stronger the entrainment. The situation is somewhat complicated by the presence of several mechanisms that impact the ion component of thrust, primarily the charge exchange and elastic ion-neutral collisions, and electron impact ionization of neutrals, but nonetheless the decrease in the ion thrust component is the key factor of the entrainment, and thus considered below.

Figure 8, right, presents the temporal change in thrust for three values of neutral density considered in this work. The results show that increase in neutral density leads to considerable decrease in ion contribution to thrust, which decreases at its peak by about 10% as the neutral density changes from 10^{18} atom/m^3 to 5×10^{18} atom/m^3, and another 25% as density goes up to 25×10^{18} atom/m^3. The decrease is less then linear due to a non-linear momentum and mass transfer during the entrainment, the threshold nature of the ionization and collisional radiative processes, and the non-linear charge exchange rate that is impacted by temperature variations shown in Fig. 7, left. Note that the introduction of neutrals only in the coreflow, as compared to the uniform injection across the chamber, is beneficial only as long as the plasma density is higher in the center, since the entrainment efficiency is governed both by neutral and plasma density. The results for a 10 eV plasma (not shown here) are quantitatively similar to the 5 eV case for all neutral densities under consideration.

VI. Conclusions

The paper presents the results of numerical modeling of neutral entrainment in a Field Reversed Configuration thruster. The numerical approach chosen is the combination of the implicit Particle-In-Cell method for modeling plasma and the direct simulation Monte Carlo method for modeling neutral particles. The multi-dimensional PIC code Celeste3D extended with a DSMC capability was used in this work to model a neon-based FRC plasmoid interacting with neon neutral gas. The modeling capability was extended as compared to the previous work to include all relevant collisional radiative processes in neon. The plasma density of 10^{18} m^{-3} and temperatures of 5 and 10 eV were assumed, with the neutral density varied between 10^{18} m^{-3} and 2.5×10^{19} m^{-3}. The computations were conducted in the reference frame of the plasmoid, with neutral gas injected in the plasmoid coreflow with a relative velocity of 20 km/s. The results cover macroparameters and distribution function, as well as thruster performance related properties.

The numerical modeling included spatially uniform thermochemical relaxation (adiabatic heat bath)

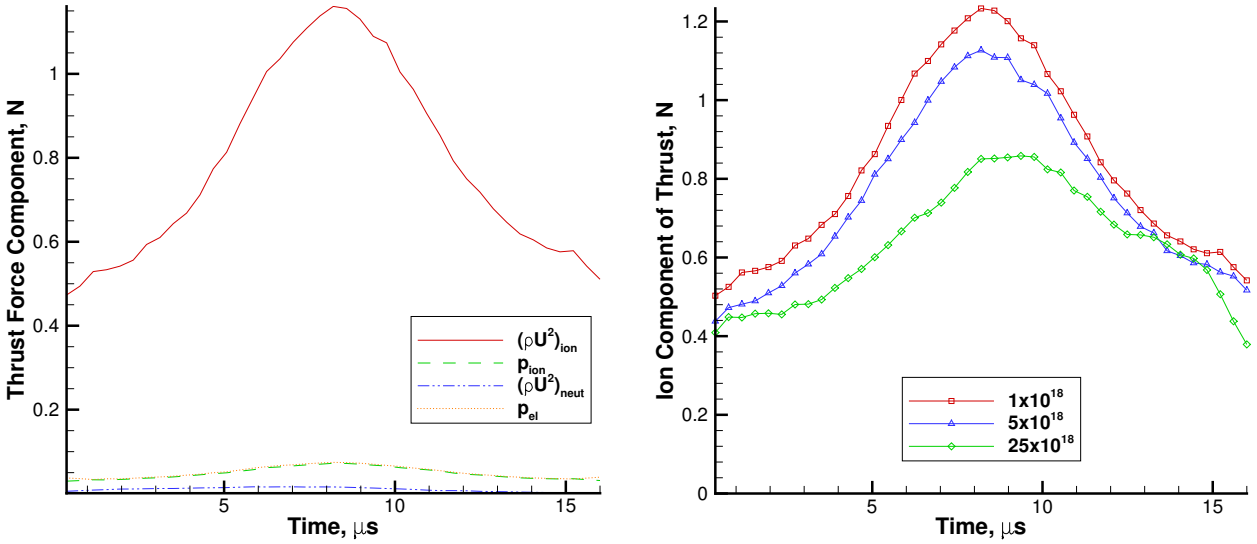

Figure 8.

with neutral and plasma properties close to those of a typical FRC thruster. The heat bath computations showed that the relaxation process proceeds under conditions of strong thermal and chemical non-equilibrium; ion, electron, and neutral temperatures strongly differ, and the ion and neutral gas distribution function is strongly non-Maxwellian. The electron velocity distribution function is close to Maxwellian when the Coulomb collisions are taken into consideration; otherwise, electron impact ionization was found to deplete high velocity tail of the electron distribution function. Electronic excitation and radiation processes were found to noticeably decrease primarily electron temperature, and the change is especially noticeable for interaction times exceeding 10μs.

Two-dimensional modeling of the FRC neutral entrainment showed strong entrainment for neutral densities exceeding 5×10^{18} m^{-3}, with momentum transfer and thruster efficiency being non-linear functions of neutral density. The probability of neutral atom collision with the plasmoid was estimated at approximately 10%, with most of the collisions being charge exchange events. Electron impact ionization is not significant for a 5 eV plasmoid, but becomes a factor at 10 eV. For neutral gas injected in a 10% area of the chamber, the ion contribution to thrust was found to decrease by up to 30% due to the plasma-neutral momentum transfer when neutral density was increased to 2.5×10^{19} m^{-3}.

VII. Acknowledgments

The work was supported by the Air Force Office of Scientific Research (Dr. Mitat Birkan). Fruitful discussions with Dr. David Kirtley are greatly appreciated.

References

[1]McKenna K.F. et al., "Particle confinement scaling in field-reversed configurations", Phys. Rev. Lett. 50, 1787 (1983)

[2]Rostoker N. and Qerushi A., "Classical transport in a field reversed configuration", Plasma Phys. Rep. 29(7), 626 (2003).

[3]Elliott F., Foster J., and Patterson M., An Overview of the High Power Electric Propulsion (HiPEP) Project, AIAA Paper 2004-3453.

[4]Kirtley D., Brown D., and Gallimore A. Details on an annular field reversed configuration plasma device for spacecraft propulsion, IEPC-2005-171.

[5]Miller S., Rovey J. Progress in modeling of pre-ionization and geometric effects on a field-reversed configuration plasma thruster, AIAA 2009-3733.

[6]Slough J., Kirtley D., and Weber T. Pulsed plasmoid propulsion: the ELF thruster, IEPC-2009-265.

[7]Brackbill J., Gimelshein S., Gimelshein N., Cambier J.-L., Ketsdever A. Ionization and Charge Exchange Reactions in Neutral Entrainment of a Field Reversed Configuration Thruster, AIAA Paper 2012-4102.

[8]Lapenta, J.U. Brackbill, Dynamic and Selective Control of the Number of Particles in Kinetic Plasma Simulations, Journal of Computational Physics, 115, 213-227, 1994.

[9]NIST ASD Team, Y. Ralchenko, A. E. Kramida, and J. Reader, NIST Atomic Spectra Database (version 3.1.5), (Online). Available: http:// www.nist.gov/asd3 (2010), National Institute of Standards and Technology, Gaithersburg, MD.

[10]Roberto S. Brusa, Grzegorz P. Karwasz, Antonio Zecca, "Analytical partitioning of total cross sections for electron scattering on noble gases", Z. Phys. D 38, 279287 (1996)

[11]Antonio Zecca, Grzegorz P Karwasz and Roberto S Brusa, "Electron scattering by Ne, Ar and Kr at intermediate and high energies, 0.5-10 keV", J. Phys. B: At. Mol. Opt. Phys. 33 (2000) 843-845.

[12]R.P.McEachran and A.D.Stauffer, Phys.Lett.A,107 No. 8 , p.397-399

[13]Bird, G.A., *Molecular Gas Dynamics and the Direct Simulation of Gas Flows.* Clarendon Press, Oxford. 458 pp, 1994.

[14]K. Nanbu and S. Yonemura, Weighted Particles in Coulomb Collision Simulations Based on the Theory of a Cumulative Scattering Angle J. Comp. Phys, 145, 639-654 (1998)

[15]S.A. Losev, S.O. Macheret, B.V. Potapkin, G.G. Chernyi, Physical and chemical processes and gas dynamics: cross sections and rate constants. Progress in Astronautics and Aeronautics, 196, AIAA, 2002.

[16]l. C. Pitchford, J. P. Boeuf, and W. L. Morgan, User-friendly Boltzmann code for electrons in weakly ionized gas, in Proceedings of the IEEE International Conference on Plasma Science, Boston, MA, 1996 (IEEE, Piscataway, NJ, 1996).

[17]Mason, N. J. and W. R. Newell, J. Phys. B: At. Mol. Phys., 20, 1357, 1987.

[18]R. O. Jung,a) Garrett A. Piech,b) M. L. Keeler,c) John B. Boffard,d) L. W. Anderson, and Chun C. Lin "Electron-impact excitation cross sections into Ne(2p 5 3p) levels for plasma applications", J Appl Phys 109, 123303

[19]Kanik, I., J. M. Ajello, and G. K. James, J. Phys. B: At. Mol. Phys. 29, 2355, 1996.

[20]C.M.Ferreira, J.Loureiro and A.Ricard, J.Appl.Phys., 57 (1985) 82

[21]Bird GA. 1979. Simulation of multi-dimensional and chemically reacting flows. *Proc. 11th Int. Symp. on Rarefied Gas Dynamics, Paris, pp.365-388*, ed. R. Campargue, Commissariat a l'Energie Atomique

[22]McGuire, E. Phys. Rev. A 20, 445 (1979)

[23]P.Ricci, G. Lapenta, J.U. Brackbill, GEM Challenge: Implicit Kinetic Simulations with the Physical Mass Ratio, Geophysical Research Letters, 29, 10.1029/2002GL015314, 2002.

[24]Lapenta, G., Brackbill, J. and Ricci, P. Phys. Plasmas 13, 055904 (2006).

[25]Gimelshein S.F., Levin D.A., Collins R.J. Modeling of Infrared Radiation in a Space Transportation System Environment. AIAA Journal, Vol. 40, No. 4, 2002, pp. 781-790.

[26]Ivanov, M.S. and Rogasinsky, S.V., Analysis of the numerical techniques of the direct simulation Monte Carlo method in the rarefied gas dynamics, *Soviet J. Numer. Anal. Math. Modeling*, Vol. 3, No. 6, 1988, pp. 453-465.

[27]J. Schmid-Burgk, Finite Amplitude Density Variations in a Self-Gravitating Isothermal Gas Layer, *Astrophysical Journal* **149**, 727-729 (1967).